OPTICAL EYE MODEL

PACS numbers: 42.66.Ct; 42.15.Fr
DOI: 10.1070/QE2008v038n11ABEH013840

Human eye aberrations: 1. Development of personalised models of the human eye optical system based on measurements

A.V. Dubinin, T.Yu. Cherezova, A.V. Kudryashov

***Abstract*. Based on experimental studies of human eye monochromatic aberrations, the eye models are proposed which take into account the individual features of eye aberrations of patients.**

Keywords: *eye model, aberrations, wavefront*.

1. Introduction

A human eye is an intricate optical instrument. It has been the subject of investigation for many years. As the new properties of the human eye were discovered, scientists attempted to develop new or improve existing human eye models. It was necessary first of all for further studies of the behaviour and properties of the human eye under different conditions, which is more convenient and safe than to study directly the living human eye.

The first human eye model, which was proposed by Huygens as early as 1702, demonstrated the presence of a turned over image on the eye retina, and it was proposed for the first time to correct aberrations by using spectacle lenses [1, 2].

However, the two human eye models proposed by Allvar Gullstrand in 1909 became really revolutionary [1 – 4]. These models represented the human eye structure most precisely. One of them simulated the human eye with the maximum accommodation, while another simulated the eye focused to infinity. Gullstrand took into account for the first time in his models the layered structure of the crystalline lens of the human eye and introduced up to six refracting media to them.

The next step in the human eye simulation was the use of aspherical surfaces. In 1985 the research group of Rafael Navarro proposed a new human eye model, which very precisely reproduced the averaged optical properties of the human eye [5]. All surfaces in this model without exception were made aspherical (Table 1). In addition, Navarro selected for the first time the media with the wavelength

Table 1. Parameters of the personalised eye models and the Navarro eye model.

	Surface	Radius/mm	Conic constant	Thic-kness/mm	Refractive index
Patient AD (right eye)	1	7.72	−0.26	0.55	1.373
	2	6.5	0	3.05	1.3343
	3	∞	0	0	–
	4	10.2	−3.00	4.0	1.4162
	5	−6.0	−1.00	16.55	1.333
	6	−12.0	0	–	–
	Pupil displacement: 0.4 mm nosally				
Patient AB (left eye)	1	7.72	−0.3	0.55	1.373
	2	6.5	0	3.05	1.3343
	3	∞	0	0	-
	4	10.2	−3.0	4.0	1.4162
	5	−6.0	−1.0	16.53	1.333
	6	−11.5	0	–	–
	Pupil displacement: 0.45 mm nosally				
Patient RL (right eye)	1	7.6	−0.28	0.55	1.373
	2	6.5	0	3.05	1.3343
	3	∞	0	0	–
	4	11.0	−3.0	4	1.4162
	5	−5.8	−1.0	16.50	1.333
	6	−11	0	–	–
	Pupil displacement: 0.6 mm nosally				
Navarro eye model	1	7.72	−0.26	0.55	1.373
	2	6.5	0	3.05	1.3343
	3	∞	0	0	–
	4	10.20	−3.1316	4.0	1.4162
	5	−6.0	−1.0	16.32	1.333
	6	−12.0	0	–	–

Notes: (1) anterior cornea surface; (2) posterior cornea surface; (3) pupil; (4) front crystalline lens surface; (5) rear crystalline lens surface; (6) retina.

A.V. Dubinin International Laser Center, M.V. Lomonosov Moscow State University, Vorob'evy gory, 119992 Moscow, Russia;
e-mail: alex_dubinin@mail.ru;
T.Yu. Cherezova Department of Physics, M.V. Lomonosov Moscow State University, Vorob'evy gory, 119992 Moscow, Russia;
e-mail: cherezova@mail.ru;
A.V. Kudryashov Shatura Branch of the Moscow State Open University, ul. Sportivnaya 9, 140700 Shatura, Moscow region, Russia;
e-mail: kud@activeoptics.ru

Received 6 March 2008
Kvantovaya Elektronika **38** (11) 1048 – 1052 (2008)
Translated by M.N. Sapozhnikov

dependences of the refractive index that were very close to the dispersion of the real human eye.

All the later models are variants of already existing models, which are based on the improved measurement methods and use modern technologies for manufacturing optical media. Among them are human eye models proposed in papers [6–9]. However, as follows from the measurements of human eye aberrations, all these models cannot explain aberrations of a particular eye measured at a fixed wavelength because they describe only averaged general properties of the human eye. In particular, the eye models have the axial symmetry, whereas the directions of the optical axis and the axis along which imaging occurs in the eye differ approximately by 5°. The aim of our study is to reproduce aberrations of an individual human eye and to develop the personalised human eye models for patients. However, before explaining the features of human eye aberrations with the help of our models, it is necessary to discuss these aberrations and methods of their measurement.

2. Experimental study of eye aberrations

It is known that the main elements of the eye, determining its optical properties, are a cornea and a crystalline lens. To simulate the optical system of the real eye, it is necessary to know the relative contributions of these two optical elements to the total eye aberrations. To determine these contributions, we studied the eye aberrations as a whole by using an aberrometer available in our lab [10]. The local wavefront tilts can be measured with this instrument by the Shack–Hartmann method [11]. Figure 1 shows the optical scheme of the experiment. A 780-nm beam from a diode laser of power no more than 30 μW is focused by the optical system of the eye on the retina, by forming a point source on it. The light scattered backward by the retina passes through all elements of the eye, acquiring total phase distortions in all these elements. The output plane of the eye is optically conjugated with the plane of the microlens raster of the Shack–Hartmann sensor. Experiments were performed with several patients, measurements being performed for each of them no less than ten times, which allowed us to calculate later the average values of Zernike polynomial coefficients and the statistical error of their measurement. During the study of aberrations of intraocular optics, a patient put on a pair of swimming goggles in which optical surfaces were replaced by high-quality plane–parallel plates (the wavefront deviation introduced by the plates did not exceed $\lambda/10$ in amplitude). The goggles were filled with a liquid for contact lens handling, which had the refractive index $n \approx 1.34$ close to that for cornea ($n = 1.37$). The difference in the refractive indices of the cornea and liquid led to the error in the estimates of Zernike polynomial coefficients, which did not exceed 10 % of their amplitude. This was taken into account in calculations of the experimental error.

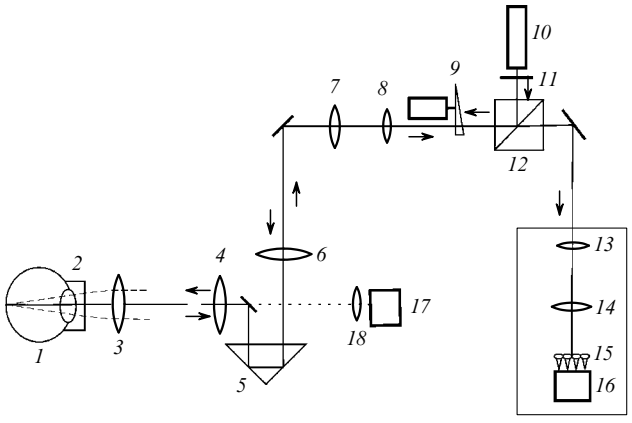

Figure 1. Scheme of the aberrometer: (*1*) patient eye; (*2*) goggles filled with liquid; (*3*) lens for hypermetropia compensation; (*4*) ($f = 50$ mm), (*6*) ($f = 50$ mm), (*7*) ($f = 50$ mm), (*8*) ($f = 20$ mm), (*13*) ($f = 20$ mm), (*14*) ($f = 20$ mm), (*18*) ($f = 3$ mm) converging lenses; (*5*) movable prism (isosceles 15×20 mm); (*9*) rotating wedge (40 mm in diameter, 0.5°); (*10*) 780-nm, 2mW LM-780-2AB semiconductor laser (the beam diameter is 0.8 mm); (*11*) NS2 filter; (*12*) 50/50 beamsplitter cube (12.5×12.5 mm); (*15*) lens raster (20×20 microlenses of diameter 0.3 mm, $f = 8$ mm); (*16*) Basler A602f CCD camera; (*17*) Artcam-130MI-NIR-OR CCD camera.

Thus, the Zernike polynomial coefficients for the cornea were determined by subtracting coefficients for intraocular optics from the corresponding total coefficients for the eye. When the cornea refraction was compensated by this method, the optical power of the eye considerably decreased, i.e. the eye became far-sighted. The eye hypermetropia was compensated with the help of an additional high-quality lens for which the Zernike polynomial coefficients, except defocusing, did not exceed $\lambda/10$ (Fig. 1).

The presence of the swimming goggles and compensating lens did not allow the eye centring with the help of a special camera [(*17*) in Fig. 1]. Because of this, the eye position in a plane perpendicular to the instrument axis was directly controlled by centring a hartmannogram on the Shack–Hartmann sensor camera.

Figure 2 presents the interferograms of the wavefront corresponding to the intraocular optics, cornea and eye as a whole, which were calculated based on the experimental results obtained for one of the patients (interferograms are presented by neglecting defocusing). One can see that the root-mean-square deviation of the wavefront corresponding the eye placed into immersion liquid was 0.48 μm, while these deviations corresponding to the cornea and the eye as a whole were 0.36 and 0.28 μm, respectively. These data show that aberrations of the crystalline lens and cornea for the eye of this patient considerably exceed the total aberrations of the eye and compensate each other to a great extent.

Figure 3 presents the Zernike polynomial coefficients for three patients AB, AD, and RL. The coefficients were averaged over ten measurements. One can see, for example, that these coefficients for the cornea and crystalline lens for patient AB have the same absolute value but opposite signs, while a curve corresponding to total coefficients for the eye is located between the curves corresponding to the crystalline lens and cornea and passes near zero. The result obtained for patient AD is similar. The same picture was also observed for patient RL, however, mainly for higher-order coefficients.

The results of the measurements confirm the fact that aberrations of the optical system of the eye as a whole are weaker than individual aberrations of the crystalline lens and cornea. These two elements are combined to minimise the total eye aberrations, thereby increasing the visual acuty. However, for some patients, for example, patient RL this

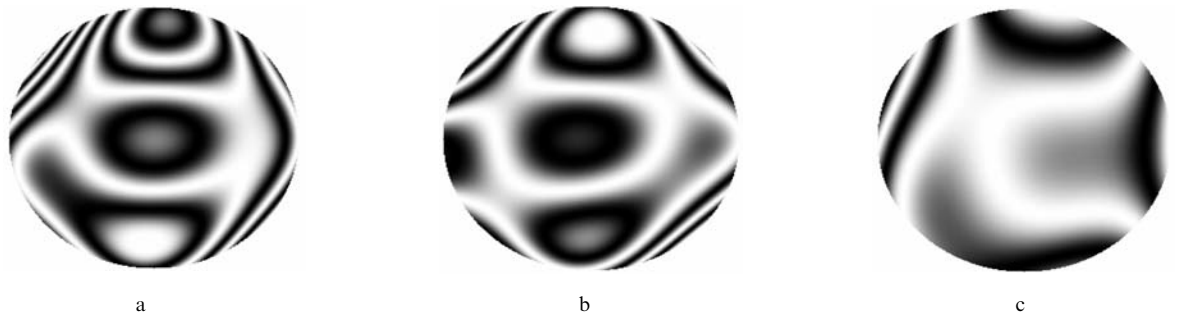

a b c

Figure 2. Interferograms of the wavefront for the intraocular optics (a), cornea (b) and eye of an inspected patient.

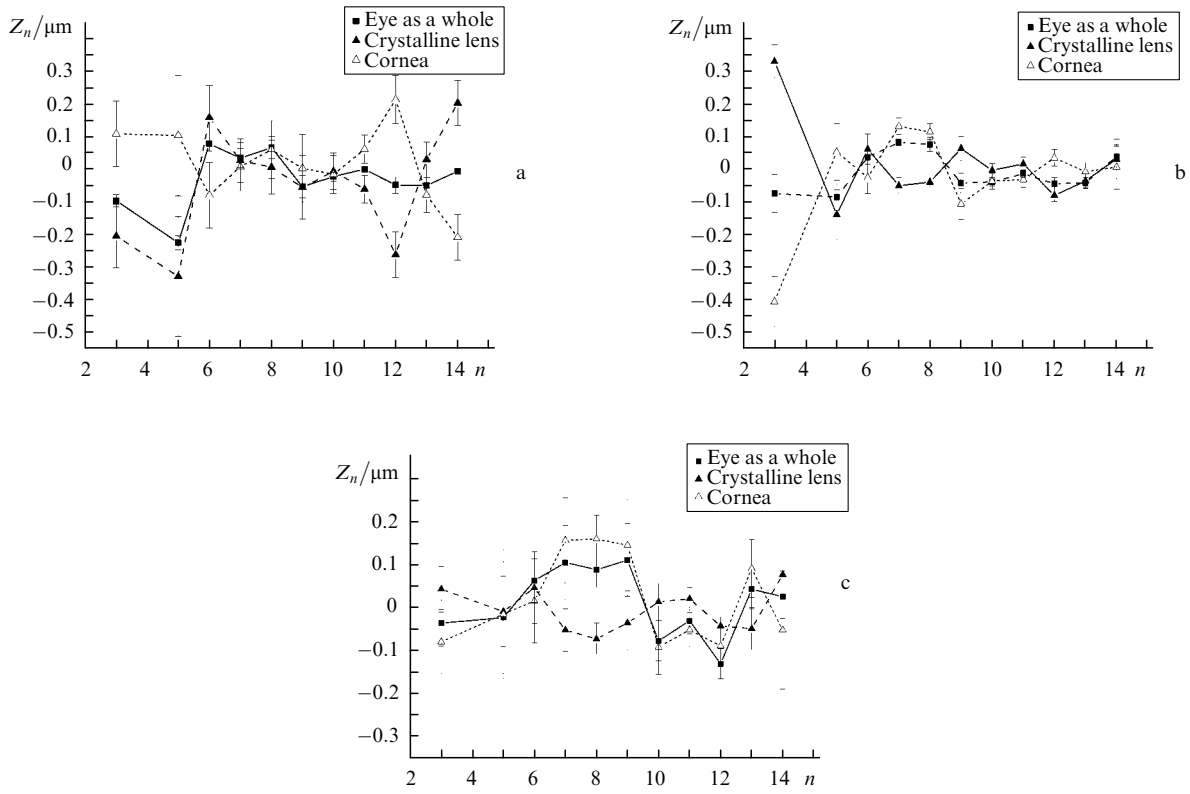

Figure 3. Dependences of the Zernike polynomial coefficients Z_n on the polynomial number n for patients AB (a), AD (b), and RL (c).

balance can be violated, resulting in the general deterioration of vision.

This result explains indirectly the appearance of higher-order aberrations upon implantation of an intraocular lens into the optical system of the eye by the violation of the balance caused by implantation. The results of this experiment also show that, for example, an operation of laser correction of vision should be performed by taking into account the aberrations of the crystalline lens and cornea separately rather than by considering total aberrations of the eye as a whole, as is done in modern systems. It is this approach that will prevent the appearance of post-surgical complications caused by higher-order aberrations.

To simulate the optical system of the eye, it is also necessary to know its off-axial aberrations. Below, we consider the study of these aberrations. Measurements were performed by using the modified variant of the experimental setup shown in Fig. 4. Aberrations along different directions were studied by placing beamsplitter (*1*) in front of the eye, which transmited 92 % of the

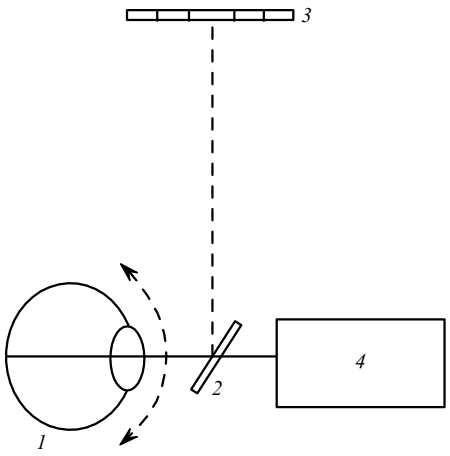

Figure 4. Modified experimental setup for measuring off-axial eye aberrations: (*1*) patient eye; (*2*) beamsplitter; (*3*) target; (*4*) aberrometer.

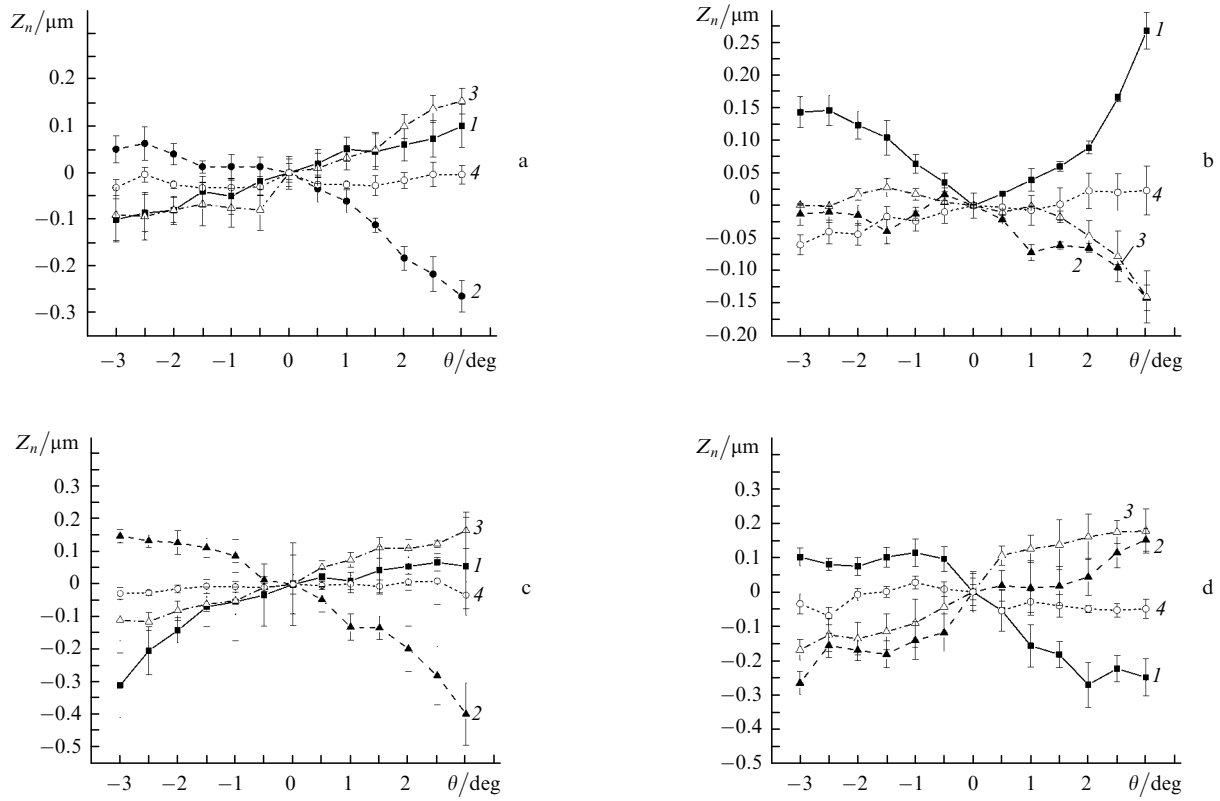

Figure 5. Zernike polynomial coefficients Z_2^0 (*1*), Z_2^{-2} (*2*), Z_3^1 (*3*), and Z_4^0 (*4*) for the right eyes of patients AB (a), AD (b), RL (c), and AK (d).

incident light at 780 nm and reflected 8 % of light. By using the beamsplitter, a patient could focus his eye to different marks inscribed on a target and located at an angle distance of 0.5° from each other along the horizontal line, thereby turning the eye in the horizontal plane. For patient's convenience, the required mark on the target was illuminated by a red diode, which provided a more precise fixation of the eye. In this case, according to the diode position, the axis, along which the eye was fixed, was turned, which resulted in the appearance of reference sources in different regions of the eyeground. The scattered radiation from these sources was analysed with the Shack–Hartmann sensor.

The structure of retina photoreceptors is inhomogeneous, which can affect the relation between the incident radiation components reflected and scattered from the retina. To be certain that the difference of the wavefront tilts along different directions is caused namely by aberrations of the optical elements of the eye rather than the relation between the reflected and scattered components of a signal being measured [12], we formed point sources at the central part of the retina (where the structure of photoreceptors was homogeneous), i.e. at an angular distance no more than 3° from the centre. The diameter of the input light beam was 1.5–2 mm.

Figure 5 presents the Zernike polynomial coefficients measured for different angular coordinates θ of a reference source (from −3° to 3°) for the right eyes of four patients AB, AD, RL, and AK. Among four patients, a considerable defocusing on the axis (−1.7D) was observed only for patient RL, while refraction for three other patients was close to normal (−0.5D, +0.3D and −0.3D for patients AD, AB, and AK). Figure 5 presents four Zernike polynomial coefficients: Z_2^0 (defocusing), Z_2^{-2} (astigmatism), Z_3^1 (coma), and Z_4^0 (spherical aberration). To demonstrate clearly the angular dependence of the coefficients, we assumed that all the coefficients are zero for $\theta = 0$.

One can see from Fig. 5 that the change in the wavefront shape is mainly determined by second-order aberrations (astigmatism and defocusing), whereas coefficients characterising other higher-order aberrations did not change within the experimental error. Variations in the coefficients corresponding to the vertical and horizontal coma did not exceed 0.25 μm, although this type of distortions also caused some changes in the wavefront shape. Astigmatism was the main aberration determining variations in the wavefront shape for patients RL and AB (the coefficient corresponding to this aberration was 0.5 and 0.3 μm,

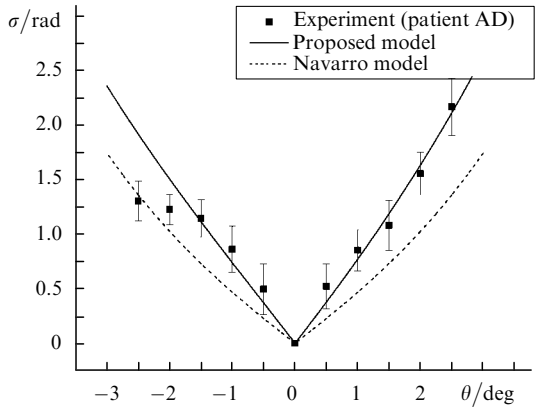

Figure 6. Dependences of the residual correction error σ on the position of a retina point being imaged (patient AD, right eye).

a b

Figure 7. Experimental interferogram (a) and interferogram (b) obtained with the help of the personalised eye model, which characterise aberrations on the axis of the right eye of patient AD.

respectively). The coefficient corresponding to defocusing for patients AD, RL, AN, and AK was 0.3, 0.3, 0.2, and 0.3 μm, respectively.

Thus, off-axial optical distortions of the image in the eye are determined by low-frequency aberrations in the spatial spectrum. These distortions are different for different patients, which is caused by the individual properties of the optical system of the eye of each of them and requires special modelling of the eyes of patients.

3. Human eye modelling

Our next task was to develop human eye models describing correctly eye aberrations for each of the patients being inspected. Our models were based on the Navarro model (see Table 1). This model reproduces best of all aberrations for angles $\sim 10^\circ - 15^\circ$ [13].

Our aim was to construct a simple model of the eye, in which off-axial and axial aberrations would qualitatively coincide with experimental data. Simulations were performed by using the ZEMAX software package. We simulated the optical system of a particular eye by varying the radius of curvature of surfaces and the values of conic constants to obtain variations of off-axial aberrations that would qualitatively reproduce experimental results obtained for each particular eye. We also took into account the possible displacement of the pupil centre with respect to the eye axis by a distance of ~ 0.5 mm [8]. We tried to obtain the coincidence of the ratio of Zernike polynomial coefficients for the crystalline lens and cornea with experimental results obtained for each patient. We found the dependence of the root-mean-square deviation of the wavefront from the reference source position, which coincided with the experimental dependence within the measurement accuracy (Fig. 6).

To obtain the specified relation between the coefficients characterising aberrations of the optical elements of the eye on its axis, we introduced additionally the bendings of the cornea and crystalline lens surfaces. Figure 7 presents interferograms calculated for measured axial aberrations and axial aberrations reproduced by the model. One can see that the measured and reproduced aberrations almost completely coincide. The parameters of the personalised eye models for inspected patients are presented in Table 1.

Thus, the eye models proposed in our paper describe within the measurement accuracy the axial and off-axial aberrations of the eyes of patients and the relation between contributions from different optical elements of the eye into total eye aberrations. Such models explain the properties of eye aberrations for inspected patients and differ from the known eye models by the values of conic constants, the curvature of surfaces of optical elements and by the pupil displacement (see Table 1).

4. Conclusions

We have studied off-axial and axial aberrations and the contribution of the cornea surface and intraocular optics to total eye aberrations. Based on the experimental data obtained in the study, the personalised models of the eyes of inspected patients have been developed.

These models have axial and off-axial aberrations and relation between contributions from different optical elements of the eye to total eye aberrations that are specific for each of the patients.

References

1. Mouroulis P. (Ed.) *Visual Instrumentation: Optical Design and Engineering Principles* (New York: Mcgraw-Hill, 1999).
2. Duke-Elder S., Abrams D. *System of Ophtalmology* (StLouis: Mosby, 1970).
3. Gullstrand A., in *Physiological Optics* (Hamburg: Voss, 1909) pp 350 – 358.
4. Gullstrand A., in *Nobel Lecture, Physiology or Medicine 1901–1921* (Amsterdam: Elsevier, 1967).
5. Navarro R., Santamaria J., Bescos J. *J. Opt. Soc. Am. A*, **2**, 1273 (1985).
6. Thibos L.N., Ye M., Zhang X., Bradley A. *Appl. Opt.*, **31**, 3594 (1992).
7. Schwiegerling J. *Field Guide to Visual and Ophtalmic Optics* (Washington: SPIE Press, 2004).
8. Liou H.L., Brennan N.A. *J. Opt. Soc. Am. A*, **14**, 1684 (1997).
9. Siedlecki D., Kasprzak H., Pierscionek B.K. *Opt. Lett.*, **29**, 1197 (2004).
10. Galetskiy S., Letfullin R., Dubinin A., Cherezova T., Belyakov A., Kudryashov A. *Proc. SPIE Int. Soc. Opt. Eng.*, **6018**, 601806 (2005).
11. Prieto P.M., Vargas-Martin F., Goelz S., Artal P. *J. Opt. Soc. Am. A*, **17**, 1388 (2000).
12. Delori F.C., Pflibsen K.P. *Appl. Opt.*, **28**, 1061 (1989).
13. Escudero-Sanz I., Navarro R. *J. Opt. Soc. Am. A*, **16**, 1881 (1999).